


Article

Optimal Configuration of Electricity-Heat Integrated Energy Storage Supplier and Multi-Microgrid System Scheduling Strategy Considering Demand Response

Yuchen Liu ¹, Zhenhai Dou ^{1,*} , Zheng Wang ¹, Jiaming Guo ¹, Jingwei Zhao ² and Wenliang Yin ¹

¹ School of Electrical and Electronic Engineering, Shandong University of Technology, Zibo 255000, China; 13706383106@163.com (Y.L.); 22504040047@stumail.sdut.edu.cn (Z.W.); gjm000629@163.com (J.G.); yinwenliang@sdut.edu.cn (W.Y.)

² State Power Investment Corporation Haiyang Offshore Wind Power Co., Ltd., Guangzhou 510710, China; zhaojingwei98@163.com

* Correspondence: douzhenhai@sdut.edu.cn

Abstract: Shared energy storage system provides an attractive solution to the high configuration cost and low utilization rate of multi-microgrid energy storage system. In this paper, an electricity-heat integrated energy storage supplier (EHIESS) containing electricity and heat storage devices is proposed to provide shared energy storage services for multi-microgrid system in order to realize mutual profits for different subjects. To this end, electric boiler (EB) is introduced into EHIESS to realize the electricity-heat coupling of EHIESS and improve the energy utilization rate of electricity and heat storage equipment. Secondly, due to the problem of the uncertainty in user-side operation of multi-microgrid system, a price-based demand response (DR) mechanism is proposed to further optimize the resource allocation of shared electricity and heat energy storage devices. On this basis, a bi-level optimization model considering the capacity configuration of EHIESS and the optimal scheduling of multi-microgrid system is proposed, with the objectives of maximizing the profits of energy storage suppliers in upper-level and minimizing the operation costs of the multi-microgrid system in lower-level, and solved based on the Karush-Kuhn-Tucker (KKT) condition and Big-M method. The simulation results show that in case of demand response, the total operation cost of multi-microgrid system and the total operation profit of EHIESS are 51,687.73 and 11,983.88 CNY, respectively; and the corresponding electricity storage unit capacity is 9730.80 kWh. The proposed model realizes the mutual profits of EHIESS and multi-microgrid system.

Keywords: multi-microgrid system; electricity-heat integrated energy storage supplier; demand response; bi-level optimization model



Citation: Liu, Y.; Dou, Z.; Wang, Z.; Guo, J.; Zhao, J.; Yin, W. Optimal Configuration of Electricity-Heat Integrated Energy Storage Supplier and Multi-Microgrid System Scheduling Strategy Considering Demand Response. *Energies* **2024**, *17*, 5436. <https://doi.org/10.3390/en17215436>

Academic Editors: Bingtuan Gao, Xiaofeng Liu and Lixia Sun

Received: 20 September 2024

Revised: 28 October 2024

Accepted: 29 October 2024

Published: 31 October 2024



Copyright: © 2024 by the authors. Licensee MDPI, Basel, Switzerland. This article is an open access article distributed under the terms and conditions of the Creative Commons Attribution (CC BY) license (<https://creativecommons.org/licenses/by/4.0/>).

1. Introduction

In recent years, with the overuse of fossil energy and the increase of greenhouse gas emissions, the energy crisis as well as the climate warming is intensified. The development of traditional electricity industry is limited by conditions such as the environment and resources, and is in urgent need of transformation [1,2]. Meanwhile, renewable energy generation such as wind power and photovoltaic are developing rapidly, and the penetration rate of renewable energy is increasing, which brings certain challenges to the stable operation of power system [3,4]. Microgrid stand to meet these challenges by virtue of their renewable energy consumption capacity and flexibility. With the growing market size of microgrid, the demand for microgrid construction and renovation has gradually increased. Individual microgrid faces the problem of high operation cost. To this end, the concept of multi-microgrid system has emerged [5,6]. Multi-microgrid system can optimize the distribution of resources and benefits among different subjects by interconnecting with the upper-level grid, effectively compensating for the impact of randomness and volatility

of distributed energy sources on the system, and further improving the energy utilization rate and the stability of system operation [7,8]. Ref. [9] constructs a multi-microgrid system to address load demand variations due to the stochastic character of renewable energy generation. Ref. [10] achieves multi-energy complementary co-optimization in multi-microgrid systems and proposes a benefit distribution strategy balancing fairness and stability. Ref. [11] uses a two-layer optimization structure for multi-microgrid system day-ahead and real-time energy scheduling, respectively, where energy interactions between adjacent microgrids reduce the total operation cost. In Ref. [12], the planning problem of multi-microgrid system coupled with electricity, heat and hydrogen is studied, which significantly reduces carbon emissions and environmental pollution. Ref. [13] specifically addresses the optimization of the design and operation of islanded multi-microgrid system, using a column and constraint generation based approach to address both the design and operation phases. Energy storage equipment can be used to solve the problem of time inconsistency between renewable energy generation and load demand [14]. However, configuring separate energy storage system for each microgrid can significantly increase the construction cost, and the utilization rate of the corresponding energy storage is low. Accordingly, shared energy storage has become a hot research topic for the past few years.

Shared energy storage has become a more attractive way of energy storage configuration in multi-microgrid system by virtue of its flexibility and economic advantages, which makes up for the regulation needs on the microgrid side and ensures the stable operation of renewable energy power system [15,16]. Currently, the research on shared energy storage is mainly distributed in the planning of energy storage capacity and the optimization of operation mode [17]. Ref. [18] presents a shared energy storage capacity planning model for multi-microgrid system considering PV generation accommodation and loading capacity, and obtains a better economic return. Ref. [19] proposes a market game model for peer-to-peer (P2P) energy trading between residential user side and shared energy storage configuration, which allocates the optimal energy storage capacity with considering the competition between users, and the obtained results achieve a further reduction of energy costs. Ref. [20] proposes a business model of shared energy storage in data center cluster and considers the uncertainty of renewable energy output, which effectively reduce the investment of energy storage unit, and promote the consumption of renewable energy. Ref. [21] considers shared energy storage to provide storage capacity leasing services for large-scale photovoltaic base stations, and solves a two-stage joint optimization problem for capacity planning and operation cost optimization. The optimization results achieve coordinated operation and cost sharing between shared energy storage and base station. Studies mentioned above have thoroughly studied the configuration and operation of shared electricity energy storage services. However, users not only have electricity load demand, but their demand for heat, especially in winter, is still a non-negligible part. The high-frequency use of heating equipment in winter further increases the users' need for thermal energy storage. Refs. [22–24] focus on the application of shared thermal energy storage. Ref. [22] combines the advantages of distributed and centralized structures of energy storage system, and proposes an optimal scheduling model for an integrated energy microgrid system containing electricity and thermal storage unit, which minimizes the waste of electricity and thermal energy and obtains the optimal economic benefits. In Ref. [23], three different configurations of combined heat and power units are set up with multiple energy storage units, which improve energy utilization while reducing production costs and carbon emissions. Ref. [24] set up a hybrid power system containing wind-photovoltaic-battery-thermal energy storage, which utilizes the economic benefits and working flexibility of thermal storage units and batteries to improve the intermittently output of renewable energy. Shared electricity and thermal storage units are considered as independent devices in the above literatures, but the coupling characteristic of electricity and thermal energy in them is neglected. For shared energy storage system, the realization of the coupling of electricity and thermal energy can further enhance their flexibility and economic efficiency.

Most studies mentioned above focus on the optimization of the energy supply side problem, while the independence of users on the load side is rarely included. Load fluctuations during the actual electricity consumption by users can also affect the stable operation of the multi-microgrid system [25]. In order to maximize the profits of microgrid users, Ref. [26] proposes a novel demand response model considering the different electricity consumption behaviors of different customers during peak and valley periods, and a new algorithm called hybrid hybrid crow search algorithm—jaya algorithm (CSAJAYA) is proposed, which verifies that the demand response has a positive effect on the reduction of the system's power generation cost. Ref. [27] addresses the problem of sudden energy interruptions in an islanded microgrid by proposing a novel energy management tool for isolating the microgrid and incorporating demand response program, which ultimately reduces the system operation cost by 3% and increases the allowed cumulative faults by 13 h. Ref. [28] proposes an optimal scheduling model with combined cooling heating and power (CCHP) and carbon capture devices considering demand response, which reduces the carbon emissions of the system as well as the energy purchases of users through the dual optimization of the demand response mechanism and the carbon trading mechanism, thus contributing significantly to the protection of the environment and the reduction of costs. The user-side uncertainties make the actual operation of multi-microgrid system difficult to predict, which usually leads to difficulties in optimizing the configuration of shared energy storage system as expected, and in many cases with low utilization of the storage equipment.

Based on the summary of existing literature in Table 1, we note that: (1) Multi-microgrid system is acknowledged for its ability to consume renewable energy and flexibility of operation. Energy storage device can solve the problem of temporal inconsistency between renewable energy generation and load demand, but configuring separate storage systems for each microgrid leads to the high cost and low utilization problem. (2) Although various studies have been conducted on the configuration and optimization of shared energy storage, there is still a lack of research on the synergistic utilization of shared electricity and thermal storage unit, especially ignoring the coupling of electricity and thermal energy therein. (3) Uncertainty on the user side makes the actual operation of multi-microgrid system difficult to predict, which usually leads to difficulties in optimizing the configuration of shared energy storage system as expected, and in many cases the utilization of energy storage devices is low. In response to the research gaps presented above, this paper makes the following significant contributions:

Table 1. Details of the proposed problem of this paper compared to other studies.

Reference	Multi-Microgrid System	Shared Energy Storage Electricity/Heat/Coupling	Demand Response	Objective Storage Configuration/Operation Optimization
[11]	✓	×/×/×	✓	×/✓
[20]	×	✓/×/×	×	×/✓
[21]	×	✓/×/×	×	✓/✓
[22]	✓	✓/✓/×	×	×/✓
[24]	×	✓/✓/×	×	×/✓
[26]	✓	×/×/×	✓	×/✓

(1) An electricity-heat integrated energy storage supplier (EHIESS) specialized in providing electricity and heat storage services for multi-microgrid system is proposed. A bi-level planning model considering EHIESS capacity configuration and optimal operation of multi-microgrid system is established, and solved based on Karush-Kuhn-Tucker (KKT) condition and Big-M method.

(2) Electric boiler (EB) is introduced into EHIESS and leverages its electricity-heat coupling characteristics to realize the enhancement of the integrated electricity-heat efficiency of EHIESS. As well, the economic benefits of multi-microgrid system and EHIESS are maximized.

(3) Aiming at the volatility of user-side loads, a price-based load demand response mechanism is introduced into multi-microgrid system to dynamically regulate the loads and improve the utilization rate of shared energy storage equipment.

The rest of the paper is organized as follows. Section 2 introduces the multi-microgrid system model considering EHISS. Section 3 introduces the price-based DR model. In Section 4, the simulation analysis is carried out. Finally, the main conclusions are summarized in Section 5.

2. Multi-Microgrid System Model Sharing EHISS

2.1. Electricity-Heat-Gas Coupled Microgrid Model

The microgrid model constructed in this paper is shown in Figure 1, which consists of photovoltaic, wind turbine, CCHP, electric refrigerator, and electricity, heat and cooling loads. The microgrid model is connected to the upper energy grid (upstream network and natural gas grid). CCHP unit consists of gas turbine, gas boiler, waste heat boiler (WHB), heat exchange and lithium bromide absorption chiller (LBAC). In this section, the mathematical model of each device in the microgrid is presented as follows.

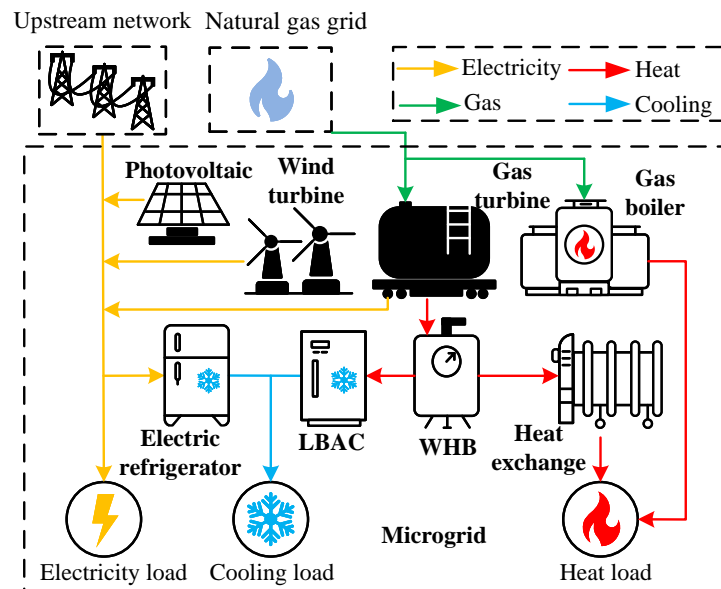


Figure 1. Topology of electricity-heat-gas coupled microgrid.

2.1.1. Combined Cooling Heating and Power

CCHP refers to the joint production of three different forms of energy for electricity, heat and cooling. CCHP provides a cost-effective way to increase energy utilization and improve environmental issues [29].

In CCHP, gas turbine generates electricity and heat by consuming natural gas. The electricity generated is used to supply electricity loads and the heat is processed by WHB and ultimately delivered to LBAC and heat exchange. The electricity and heat generated by gas turbine can be expressed as:

$$P_{GT}^{t,i} = \eta_{GT} \cdot L_{gas} \cdot V_{GT}^{t,i} \quad (1)$$

$$Q_{GT}^{t,i} = \gamma_{GT} \cdot P_{GT}^{t,i} \quad (2)$$

where $P_{GT}^{t,i}$ and $Q_{GT}^{t,i}$ are the electricity and heat generated by gas turbine in microgrid i (MG i) during hour t , respectively; η_{GT} and γ_{GT} are the electricity and heat generation efficiency of gas turbine, respectively; L_{gas} is the heat value of natural gas, which is taken as 9.7 kWh/m^3 ; $V_{GT}^{t,i}$ is the gas consumption volume of gas turbine in MG i during hour t .

Gas boiler can be used as a heat generation device in conjunction with gas turbine, and all heat it generates is used to supply the heat load. The heat generated by gas boiler in MG i during hour t , $Q_{GB}^{t,i}$, can be calculated according to the following equation:

$$Q_{GB}^{t,i} = \eta_{GB} \cdot L_{\text{gas}} \cdot V_{GB}^{t,i} \quad (3)$$

where η_{GB} is the heat generation efficiency of gas boiler; $V_{GB}^{t,i}$ is the gas consumption volume of gas boiler in MG i during hour t .

In CCHP, WHB can recycle the waste heat generated by gas turbine, and then deliver the resulting heat to heat exchange and LBAC, which can be expressed as:

$$Q_{WHB}^{t,i} = \eta_{WHB} \cdot Q_{GT}^{t,i} \quad (4)$$

where $Q_{WHB}^{t,i}$ is the heat absorbed by WHB in MG i during hour t ; η_{WHB} is the heat absorption efficiency of WHB.

Heat exchange and LBAC can convert heat energy delivered by WHB to generate heat energy and cooling energy for users, respectively. The model of heat exchange and LBAC can be formulated as follows:

$$Q_{HE}^{t,i} = \eta_{HE} \cdot \alpha \cdot Q_{WHB}^{t,i} \quad (5)$$

$$Q_{AC}^{t,i} = \eta_{AC} \cdot (1 - \alpha) \cdot Q_{WHB}^{t,i} \quad (6)$$

where $Q_{HE}^{t,i}$ is the heat output of heat exchange in MG i during hour t ; $Q_{AC}^{t,i}$ is the cooling output of LBAC in MG i during hour t ; η_{HE} and η_{AC} are the energy utilization rates of heat exchange and LBAC, respectively; α is the proportion of heat energy supplied to heat exchange by WHB.

2.1.2. Electric Refrigerator

Electric refrigerator, as a commonly used refrigeration equipment, supplies cooling load by consuming electricity. The cooling power generated by electric refrigerator in MG i during hour t , $Q_{ER}^{t,i}$, can be calculated according to the following equation:

$$Q_{ER}^{t,i} = \eta_{ER} \cdot P_{ER}^{t,i} \quad (7)$$

where $P_{ER}^{t,i}$ is the power consumption of electric refrigerator in MG i during hour t ; η_{ER} is the cooling efficiency of electric refrigerator.

2.2. Electricity-Heat Integrated Energy Storage Supplier Model

EHISS forms a bi-level structure with multi-microgrid system, which can calculate the required capacity of energy storage equipments and the charging and discharging electricity and heat according to the energy consumption of multi-microgrid users, and carry out the construction and maintenance of energy storage equipments, thus providing shared energy storage service for multi-microgrid system, and earning profits from the energy trading and service fees. Specifically, the input of EB enables EHISS more fully to utilize the complementarities and differences of different microgrid user loads, so that the capacity configuration of electricity and thermal storage unit is more reasonable, and to realize satisfying user's demand for energy storage capacity with less investment, and the economy of EHISS can be further improved. The electricity and thermal storage units in EHISS are connected to the multi-microgrid system through buses, and the electricity and heat interactions between microgrids are carried out through the buses, as shown in Figure 2 EHISS is connected to MG 1 to MG n ($n = 1, 2, \dots, N$), and each microgrid is connected to upstream network and natural gas grid, respectively. Microgrid users who have excess electricity and heat use the energy storage service of EHISS to store

excess electricity and heat, and the microgrid users who are short of electricity and heat are supplied with electricity and heat by EHIESS.

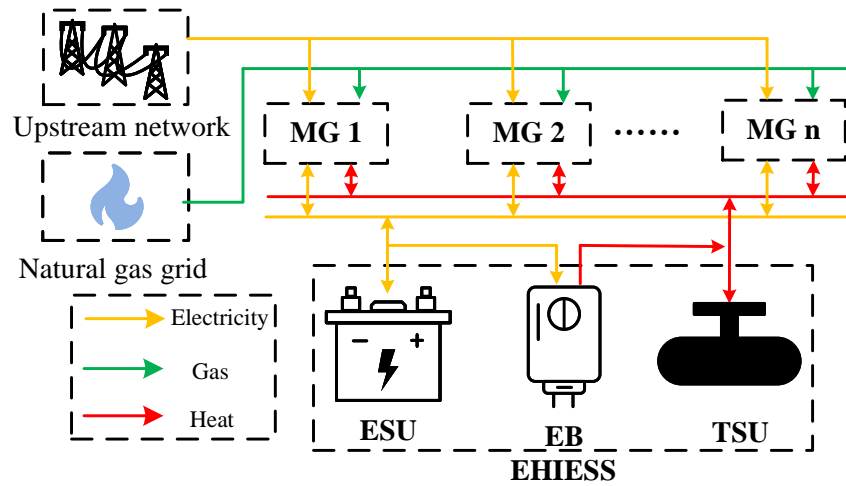


Figure 2. Multi-microgrid system shared EHIESS model.

The electricity stored in ESU during hour t , E^t , can be calculated as follows:

$$E^t = E^{t-1} + \eta_{\text{abs}} \cdot P_{\text{ch}}^{t-1} - \frac{1}{\eta_{\text{re}}} \cdot P_{\text{dis}}^{t-1} - P_{\text{EB}}^{t-1} \quad (8)$$

where η_{abs} and η_{re} are the charging and discharging efficiencies of ESU, respectively; P_{ch}^{t-1} and P_{dis}^{t-1} are the charging and discharging electricity of EHIESS during hour $t-1$, respectively; P_{EB}^{t-1} is the power consumption of EB during hour $t-1$.

The heat stored in TSU during hour t , H^t , can be calculated as follows:

$$H^t = H^{t-1} + \omega_{\text{abs}} \cdot Q_{\text{ch}}^{t-1} - \frac{1}{\omega_{\text{re}}} \cdot Q_{\text{dis}}^{t-1} + Q_{\text{EB}}^{t-1} \quad (9)$$

where ω_{abs} and ω_{re} are the heat charging and discharging efficiencies of TSU, respectively; Q_{ch}^{t-1} and Q_{dis}^{t-1} are the charging and discharging heat of EHIESS during hour $t-1$, respectively; Q_{EB}^{t-1} is the heat produced by EB during hour $t-1$.

In this paper, the initial storage capacity of the energy storage equipment is set to be 20% of the total capacity, which can be expressed as:

$$E^0 = 20\% \cdot E^{\text{max}}, H^0 = 20\% \cdot H^{\text{max}} \quad (10)$$

where E^0 and H^0 are the capacities of ESU and TSU at the initial time, respectively; E^{max} and H^{max} are the maximum capacities of ESU and TSU, respectively.

EB can connect ESU and TSU to convert heat into electricity when the heat load is high or ESU reaches its capacity limit. By incorporating EB equipment, the flexibility of EHIESS has been improved, resulting in higher profit for EHIESS. The model of EB can be expressed as follows:

$$Q_{\text{EB}}^t = \eta_{\text{EB}} \cdot P_{\text{EB}}^t \quad (11)$$

where η_{EB} is the conversion efficiency of EB.

2.3. Price-Based Demand Response

Different kinds of electricity loads have different sensitivities to the electricity price in practical work for multi-microgrid system, and the operation risk of microgrid and cost of users will increase without considering the different sensitivities of loads. Therefore, we considered the price-based DR in the load side. Price-based DR means that the upstream network guides users to use electricity reasonably by setting different electricity prices in

different time periods, so as to achieve the purpose of smoothing the load curve, reducing the system operation risk, and decreasing the user's energy cost [30].

Currently, the ways that can be modeled to reflect the user's response behavior to the price are price elasticity coefficient matrix, consumer psychology and so on. Among them, the method of price elasticity coefficient matrix can accurately reflect the response behavior of users to different electricity prices [31]. Price elasticity coefficient is an index that measures the influence of price changes to load demands. When the price changes in a certain time period, it will not only affect the demand in this time period, but also indirectly change the demand in other time periods. The price elasticity coefficient includes the self-demand elasticity coefficient and cross-elasticity coefficient.

The elements of the price elasticity matrix, $e_{t,j}$, represent the elasticity coefficients of the electricity load during hour i with respect to the price of electricity during hour j , can be calculated as follows [32]:

$$e_{t,j} = \frac{\Delta P_L^t}{P_{L,0}^t} \frac{\rho_0^j}{\Delta \rho^j} \quad (12)$$

where ΔP_L^t is the electricity load changes after DR during hour t ; $P_{L,0}^t$ is the initial electricity load; $\Delta \rho^j$ is the electricity price changes after DR during hour j ; ρ_0^j is the initial electricity price during hour j . When t equals j , $e_{t,j}$ is the self-demand elasticity coefficient, when t and j are not equal, $e_{t,j}$ is the cross-elasticity coefficient.

2.3.1. Curtailable Load

Loads are categorized into curtailable load (CL) and shiftable load (SL) based on differences in sensitivity to prices. CL can choose whether or not to engage in load curtailment by comparing the price of electricity before and after considering DR for a given time period. The changes of CL after DR during hour t is given as follows:

$$\Delta P_{CL}^t = P_{CL}^0 \left[\sum_{j=1}^{24} E_{CL}(t,j) \frac{\rho^j - \rho_0^j}{\rho_0^j} \right] \quad (13)$$

where P_{CL}^0 is the initial CL quantity; $E_{CL}(t,j)$ is the price elasticity matrix with respect of CL; ρ^j is the electricity price during hour j .

2.3.2. Shiftable Load

SL can compare the prices before and after DR and flexibly choose whether to adjust the working hours or not. Customers will shift the load from peak hours into valley hours based on the time-of-use price. The change of SL after DR during hour t is given as follows:

$$\Delta P_{SL}^t = P_{SL}^0 \left[\sum_{j=1}^{24} E_{SL}(t,j) \frac{\rho^j - \rho_0^j}{\rho_0^j} \right] \quad (14)$$

where P_{SL}^0 is the initial SL quantity; $E_{SL}(t,j)$ is the price elasticity matrix with respect of SL.

2.4. Energy Balance in Microgrid

The three types of energy flow in the microgrid, electricity, heat and cooling, should satisfy the corresponding energy balance relationship. The expression for the electrical balance of the microgrid is as follows:

$$P_{GT}^{t,i} + P_{WT}^{t,i} + P_{PV}^{t,i} + P_{grid}^{t,i} + P_{mg,b}^{t,i} = P_{mg,s}^{t,i} + P_{ER}^{t,i} + P_{el}^{t,i} \quad (15)$$

where $P_{WT}^{t,i}$ and $P_{PV}^{t,i}$ are the electricity generated by WT and PV of MG i during hour t , respectively; $P_{grid}^{t,i}$ is the electricity purchased by the MG i from the upstream network;

$P_{\text{mg,b}}^{t,i}$ and $P_{\text{mg,s}}^{t,i}$ are the electricity purchased and sold by MG i , respectively; $P_{\text{el}}^{t,i}$ is the electricity load of MG i .

The cooling balance expression for the microgrid is given below:

$$Q_{\text{ER}}^{t,i} + Q_{\text{AC}}^{t,i} = Q_{\text{cl}}^{t,i} \quad (16)$$

where $Q_{\text{cl}}^{t,i}$ is the cooling load of MG i during hour t .

The heat balance expression for the microgrid is given below:

$$Q_{\text{GB}}^{t,i} + Q_{\text{HE}}^{t,i} + Q_{\text{mg,b}}^{t,i} = Q_{\text{hl}}^{t,i} + Q_{\text{mg,s}}^{t,i} \quad (17)$$

where $Q_{\text{hl}}^{t,i}$ is the heat load of MG i during hour t ; $Q_{\text{mg,b}}^{t,i}$ and $Q_{\text{mg,s}}^{t,i}$ are the heat purchased and sold by MG i , respectively.

3. A Bi-Level Optimizing Model Considering Capacity Configuration of EHIESS and Optimal Operation of Multi-Microgrid System

In order to realize the win-win situation of multi-microgrid system and EHIESS, A bi-level optimization model is established considering capacity configuration of EHIESS and optimal operation of multi-microgrid system. The upper-level model is used to solve the optimal configuration problem of EHIESS, and the lower-level model is used to solve the optimal operation problem of multi-microgrid system. The upper-level model transfers the optimized EHEISS configuration information to the lower-level model, and then, in lower-level model, each microgrid interacts with EHIESS to optimize its own energy scheduling based on its own energy consumption and EHIESS optimal configuration information. Finally, EHIESS updates its configuration based on the microgrid's scheduling data, which ultimately satisfies the bi-level optimization model and obtains the optimal results.

3.1. Upper Level Optimization Model

3.1.1. Objective Function

The objective function of the upper-level model is to maximize the profits of EHIESS over the scheduling period, the optimization variables include the capacity configurations of ESU and TSU as well as the maximum charging and discharging power. The objective function for the upper-level model is as follows:

$$\max C_{\text{upper}} = C_{\text{buy}} - C_{\text{sale}} - C_{\text{inv}} + C_{\text{serve}} \quad (18)$$

where C_{upper} is the total profits of EHIESS; C_{buy} is the cost of purchasing energy from the multi-microgrid system; C_{sale} is the profit of selling energy to the multi-microgrid system; C_{inv} is the investment and maintenance costs of the energy storage equipment in EHIESS; C_{serve} is the service fees charged by EHIESS.

The cost of purchasing energy from the microgrid includes the costs of purchasing electricity and heat, which can be expressed as:

$$C_{\text{buy}} = \sum_{i=1}^N \sum_{t=1}^{N_T} (\lambda^t \cdot P_{\text{mg,b}}^{t,i} + \varphi^t \cdot Q_{\text{mg,b}}^{t,i}) \quad (19)$$

where N denotes the number of microgrids; N_T is the length of the scheduling period; λ^t is the price of electricity purchased from ESU during hour t ; φ^t is the price of heat purchased from TSU during hour t .

Multi-microgrid system sells electricity and heat to EHIESS to generate profits, which can be expressed as follows:

$$C_{\text{sale}} = \sum_{i=1}^N \sum_{t=1}^{N_T} (\delta^t \cdot P_{\text{mg,s}}^{t,i} + \gamma^t \cdot Q_{\text{mg,s}}^{t,i}) \quad (20)$$

where δ^t is the price of electricity sold to ESU during time t ; γ^t is the price of heat sold to TSU during hour t .

The investment and maintenance costs of ESU and TSU can be calculated as:

$$C_{inv} = \frac{\eta_p P_{es}^{max} + \eta_e E^{max}}{T_{ESU}} + C_{ESU} + \frac{\eta_q Q_{es}^{max} + \eta_h H^{max}}{T_{TSU}} + C_{TSU} \quad (21)$$

where η_p and η_e are the electricity power cost and capacity cost of ESU, respectively; P_{es}^{max} is the maximum charging and discharging power of ESU; η_q and η_h are the heat power cost and capacity cost of TSU, respectively; Q_{es}^{max} is the maximum charging and discharging heat power of TSU; T_{ESU} and T_{TSU} is the operating life of ESU and TSU, respectively; C_{ESU} and C_{TSU} is the daily maintenance cost of ESU and TSU, respectively.

The service fees gained by EHISSS from multi-microgrid system, C_{serve} , can be calculated as:

$$C_{serve} = \sum_{i=1}^N \sum_{t=1}^{N_T} \theta^t \cdot (P_{mg,b}^{t,i} + P_{mg,s}^{t,i} + Q_{mg,b}^{t,i} + Q_{mg,s}^{t,i}) \quad (22)$$

where θ^t is the price of the service fees received by EHISSS during hour t .

3.1.2. Constraints

In the upper-level, we consider the storage capacity and charging/discharging power of each scheduling period of ESU and TSU in EHISSS operation, and set the upper limit constraint of storage capacity, charging/discharging power constraint and EB power constraint. The model of ESU and TSU can be formulated as follows:

$$E^{max} = \eta_{ESU} \cdot P_{es}^{max} \quad (23)$$

$$H^{max} = \eta_{TSU} \cdot Q_{es}^{max} \quad (24)$$

The maximum capacity of ESU, E^{max} , and the maximum capacity of TSU, H^{max} , are given by Equations (23) and (24), where η_{ESU} and η_{TSU} is the energy multiplication factor of ESU and TSU, respectively.

Equations (25) and (26) are the storage capacity constraints for ESU and TSU. In order to ensure the stability, efficiency, and prolong the service life of the equipments, the state of charge (SOC) limits are set to 0.1 and 0.9, respectively.

$$10\% \cdot E^{max} \leq E^t \leq 90\% \cdot E^{max} \quad (25)$$

$$10\% \cdot H^{max} \leq H^t \leq 90\% \cdot H^{max} \quad (26)$$

The charging and discharging electricity of ESU, and the charging and discharging heat of TSU constraints during hour t can be expressed as follows:

$$0 \leq P_{ch}^t \leq U_{abs}^t \cdot P_{es}^{max}, 0 \leq P_{dis}^t \leq U_{re}^t \cdot P_{es}^{max} \quad (27)$$

$$0 \leq Q_{ch}^t \leq V_{abs}^t \cdot Q_{es}^{max}, 0 \leq Q_{dis}^t \leq V_{re}^t \cdot Q_{es}^{max} \quad (28)$$

where U_{abs}^t and U_{re}^t are the charging and discharging states of ESU, respectively. When ESU is charging during hour t , U_{abs}^t is taken as 1 and U_{re}^t is taken as 0. When ESU is discharging during hour t , U_{abs}^t is taken as 0 and U_{re}^t is taken as 1. V_{abs}^t and V_{re}^t are the charging and discharging heat states of TSU. When TSU is charging during hour t , V_{abs}^t is taken as 1 and V_{re}^t is taken as 0, when TSU is discharging during hour t , V_{abs}^t is taken as 0 and V_{re}^t is taken as 1. Charging and discharging states cannot be performed at the same time.

The electricity consumption of EB during hour t is constrained as follows:

$$P_{EB}^{\min} \leq P_{EB}^t \leq P_{EB}^{\max} \tag{29}$$

where P_{EB}^{\min} and P_{EB}^{\max} are the minimum and maximum power consumption of EB during hour t , respectively.

3.2. Lower Level Optimization Model

3.2.1. Objective Function

The objective function of the lower-level model is to minimize the operation costs of the multi-microgrid system in scheduling period. The decision variables include the power purchased from the upstream network, the output power of the equipments in CCHP, the electricity consumption of electric refrigerator and the power of the microgrids trading with EHEISS. The objective function of the lower-level model can be expressed as:

$$\min C_{\text{lower}} = C_{\text{grid}} + C_{\text{gas}} + C_{\text{buy}} - C_{\text{sale}} + C_{\text{serve}} + C_{\text{ca}}^{t,i} \tag{30}$$

where C_{grid} is the cost of electricity purchased from the upstream network; C_{gas} is the cost of purchasing natural gas, which can be expressed separately as follows:

$$C_{\text{grid}} = \sum_{i=1}^N \sum_{t=1}^{N_T} \tau_{\text{grid}}^t \cdot P_{\text{grid}}^{t,i} \tag{31}$$

$$C_{\text{gas}} = \sum_{i=1}^N \sum_{t=1}^{N_T} \tau_{\text{gas}}^t \cdot (V_{\text{GT}}^{t,i} + V_{\text{GB}}^{t,i}) \tag{32}$$

where τ_{grid}^t is the electricity price of the upstream network; τ_{gas}^t is the price of natural gas.

3.2.2. Constraints

In the multi-microgrid system scheduling model, expect for the electricity, cooling, and heat power balance constraints, the output constraints of each device such as microgrid purchase and sale power constraints are also considered. The electricity and heat sold/purchased by multi-microgrid during hour t should be the sum of the excess/insufficient energy of individual microgrid, can be expressed as follows:

$$P_{\text{dis}}^t - P_{\text{ch}}^t = \sum_{i=1}^N (P_{\text{mg,b}}^{t,i} - P_{\text{mg,s}}^{t,i}) \tag{33}$$

$$Q_{\text{dis}}^t - Q_{\text{ch}}^t = \sum_{i=1}^N (Q_{\text{mg,b}}^{t,i} - Q_{\text{mg,s}}^{t,i}) \tag{34}$$

The output constraints for each device in the microgrid are as follows:

$$\left\{ \begin{array}{l} P_{\text{GT}}^{\min} \leq P_{\text{GT}}^{t,i} \leq P_{\text{GT}}^{\max} \\ Q_{\text{AC}}^{\min} \leq Q_{\text{AC}}^{t,i} \leq Q_{\text{AC}}^{\max} \\ Q_{\text{ER}}^{\min} \leq Q_{\text{ER}}^{t,i} \leq Q_{\text{ER}}^{\max} \\ Q_{\text{GB}}^{\min} \leq Q_{\text{GB}}^{t,i} \leq Q_{\text{GB}}^{\max} \\ Q_{\text{HE}}^{\min} \leq Q_{\text{HE}}^{t,i} \leq Q_{\text{HE}}^{\max} \end{array} \right. \tag{35}$$

The power constraint for energy transfer from the upstream network to MG i during hour t is given as follow:

$$0 \leq P_{\text{grid}}^{t,i} \leq P_{\text{grid}}^{\max} \tag{36}$$

where P_{grid}^{\max} is the maximum power purchased from the upstream network.

The energy trading constraints of EHEISS and multi-microgrid system are as follows:

$$\begin{cases} 0 \leq P_{mg,s}^{t,i} \leq P_{mg}^{\max} \cdot U_{sale}^{t,i}, 0 \leq P_{mg,b}^{t,i} \leq P_{mg}^{\max} \cdot U_{buy}^{t,i} \\ 0 \leq Q_{mg,s}^{t,i} \leq Q_{mg}^{\max} \cdot V_{sale}^{t,i}, 0 \leq Q_{mg,b}^{t,i} \leq Q_{mg}^{\max} \cdot V_{buy}^{t,i} \\ U_{sale}^{t,i} + U_{buy}^{t,i} \leq 1, V_{sale}^{t,i} + V_{buy}^{t,i} \leq 1 \end{cases} \quad (37)$$

where $U_{sale}^{t,i}$ and $U_{buy}^{t,i}$ are the electricity purchase state bits of the MG i . When the MG i sells electricity to ESU, $U_{sale}^{t,i}$ is equal to 1 and $U_{buy}^{t,i}$ is equal to 0. When the MG i purchases electricity from ESU, $U_{sale}^{t,i}$ is equal to 0 and $U_{buy}^{t,i}$ is equal to 1. $V_{sale}^{t,i}$ and $V_{buy}^{t,i}$ are the heat purchase state bits of the MG i . When the MG i sells heat to TSU, $V_{sale}^{t,i}$ is equal to 1 and $V_{buy}^{t,i}$ is equal to 0. When the MG i purchases electricity from ESU, $V_{sale}^{t,i}$ is equal to 0 and $V_{buy}^{t,i}$ is equal to 1.

3.3. Solution Process

The solution process of the bi-level optimization model constructed in this paper is shown in Figure 3. It is difficult to solve the bi-level optimization problem directly because of the interaction between the upper-level model and the lower-level model. In this paper, we first construct the Lagrange function according to the objective function and constraints of the lower-level model [33], and then transform the lower-level model into the constraints of the upper-level model through the Karush-Kuhn-Tucker (KKT) optimization condition, which transforms a mixed integer linear problem into a single level nonlinear problem. Then the bi-level optimization model changes into a single level mixed integer linear problem according to the Big-M method [34]. Finally, the model is constructed under the MATLAB2021a platform and solved by invoking CPLEX and YALMIP. The specific solution procedure is shown below:

Step 1: The Lagrange function for the lower model is constructed as follows [35]:

$$\begin{aligned} \min C = & \sum_{i=1}^N \sum_{t=1}^{N_T} \Delta t \left\{ \tau_{grid}^t \cdot P_{grid}^{t,i} + \tau_{gas}^t \cdot \frac{P_{GT}^{t,i}}{\eta_{GT} L_{gas}} + \tau_{gas}^t \cdot \frac{Q_{GT}^{t,i}}{\eta_{GB} L_{gas}} + \lambda^t \cdot P_{mg,b}^{t,i} + \varphi^t \cdot Q_{mg,b}^{t,i} \right. \\ & \left. - \delta^t \cdot P_{mg,s}^{t,i} - \gamma^t \cdot Q_{mg,s}^{t,i} + \theta^t \cdot (P_{mg,b}^{t,i} + P_{mg,s}^{t,i} + Q_{mg,b}^{t,i} + Q_{mg,s}^{t,i}) \right\} + \lambda_1^{t,i} [P_{GT}^{t,i} + P_{WT}^{t,i} \\ & + P_{PV}^{t,i} + P_{grid}^{t,i} + P_{mg,b}^{t,i} - P_{mg,s}^{t,i} - P_{ER}^{t,i} - P_{el}^{t,i}] + \lambda_2^{t,i} [Q_{ER}^{t,i} + Q_{AC}^{t,i} - Q_{cl}^{t,i}] \\ & + \lambda_3^{t,i} [Q_{GB}^{t,i} + Q_{HE}^{t,i} + Q_{mg,b}^{t,i} - Q_{hl}^{t,i} - Q_{mg,s}^{t,i}] + \lambda_4^{t,i} \left[\frac{Q_{HE}^{t,i}}{\eta_{HE}} + \frac{Q_{AC}^{t,i}}{\eta_{AC}} - \eta_{WHB} \cdot Q_{GT}^{t,i} \right] \\ & + \lambda_5^{t,i} \left[P_{dis}^t - P_{ch}^t - \sum_{i=1}^N (P_{mg,b}^{t,i} - P_{mg,s}^{t,i}) \right] + \lambda_6^{t,i} \left[Q_{dis}^t - Q_{ch}^t - \sum_{i=1}^N (Q_{mg,b}^{t,i} - Q_{mg,s}^{t,i}) \right] \\ & + \mu_1^{\min} [P_{GT}^{\min} - P_{GT}^{t,i}] + \mu_1^{\max} [P_{GT}^{t,i} - P_{GT}^{\max}] + \mu_2^{\min} [Q_{AC}^{\min} - Q_{AC}^{t,i}] + \mu_2^{\max} [Q_{AC}^{t,i} - Q_{AC}^{\max}] \\ & + \mu_3^{\min} [Q_{ER}^{\min} - Q_{ER}^{t,i}] + \mu_3^{\max} [Q_{ER}^{t,i} - Q_{ER}^{\max}] + \mu_4^{\min} [Q_{GB}^{\min} - Q_{GB}^{t,i}] + \mu_4^{\max} [Q_{GB}^{t,i} - Q_{GB}^{\max}] \\ & + \mu_5^{\min} [Q_{HE}^{\min} - Q_{HE}^{t,i}] + \mu_5^{\max} [Q_{HE}^{t,i} - Q_{HE}^{\max}] - \mu_6^{\min} \cdot P_{grid}^{t,i} + \mu_6^{\max} [P_{grid}^{t,i} - P_{grid}^{\max}] \\ & - \mu_7^{\min} \cdot P_{mg,s}^{t,i} + \mu_7^{\max} [P_{mg,s}^{t,i} - P_{mg}^{\max} \cdot U_{sale}^{t,i}] + \mu_8^{\min} \cdot P_{mg,b}^{t,i} + \mu_8^{\max} [P_{mg,b}^{t,i} - P_{mg}^{\max} \cdot U_{buy}^{t,i}] \\ & + \mu_9^{\max} [V_{sale}^{t,i} + V_{buy}^{t,i} - 1] - \mu_{10}^{\min} \cdot Q_{mg,s}^{t,i} + \mu_{10}^{\max} [Q_{mg,s}^{t,i} - Q_{mg}^{\max} \cdot V_{sale}^{t,i}] + \mu_{11}^{\min} \cdot Q_{mg,b}^{t,i} \\ & + \mu_{11}^{\max} [Q_{mg,b}^{t,i} - Q_{mg}^{\max} \cdot V_{buy}^{t,i}] + \mu_{12}^{\max} [V_{sale}^{t,i} + V_{buy}^{t,i} - 1] \end{aligned} \quad (38)$$

Step 2: Based on the constructed Lagrange function (38) and the complementary relaxation conditions of the lower-level model, the lower-level model can be transformed into an additional constraint for the upper model, given as follows:

$$\left\{ \begin{array}{l} \tau_{\text{grid}}^t + \lambda_1^{t,i} + \mu_6^{\text{max}} - \mu_6^{\text{min}} = 0 \\ \frac{\tau_{\text{gas}}^t}{\eta_{\text{GT}} L_{\text{gas}}} + \lambda_1^{t,i} + \mu_1^{\text{max}} - \mu_1^{\text{min}} = 0 \\ \frac{\tau_{\text{gas}}^t}{\eta_{\text{GB}} L_{\text{gas}}} - \lambda_4^{t,i} \cdot \eta_{\text{WHB}} = 0 \\ \lambda^t + \theta^t + \lambda_1^{t,i} - \lambda_5^{t,i} + \mu_8^{\text{max}} - \mu_8^{\text{min}} = 0 \\ \varphi^t + \theta^t + \lambda_3^{t,i} - \lambda_6^{t,i} + \mu_{11}^{\text{max}} - \mu_{11}^{\text{min}} = 0 \\ -\delta^t + \theta^t - \lambda_1^{t,i} - \lambda_5^{t,i} + \mu_7^{\text{max}} - \mu_7^{\text{min}} = 0 \\ -\gamma^t + \theta^t - \lambda_3^{t,i} - \lambda_6^{t,i} + \mu_{10}^{\text{max}} - \mu_{10}^{\text{min}} = 0 \\ \lambda_2^{t,i} + \frac{\lambda_4^{t,i}}{\eta_{\text{AC}}} + \mu_2^{\text{max}} - \mu_2^{\text{min}} = 0 \\ \lambda_2^{t,i} + \mu_3^{\text{max}} - \mu_3^{\text{min}} = 0 \\ \lambda_3^{t,i} + \mu_4^{\text{max}} - \mu_4^{\text{min}} = 0 \\ \lambda_3^{t,i} + \frac{\lambda_4^{t,i}}{\eta_{\text{HE}}} + \mu_5^{\text{max}} - \mu_5^{\text{min}} = 0 \\ -\mu_7^{\text{max}} \cdot P_{\text{mg}}^{\text{max}} + \mu_9^{\text{max}} = 0 \\ -\mu_8^{\text{max}} \cdot P_{\text{mg}}^{\text{max}} + \mu_9^{\text{max}} = 0 \\ -\mu_{10}^{\text{max}} \cdot Q_{\text{mg}}^{\text{max}} + \mu_{12}^{\text{max}} = 0 \\ -\mu_{11}^{\text{max}} \cdot Q_{\text{mg}}^{\text{max}} + \mu_{12}^{\text{max}} = 0 \end{array} \right. \quad (39)$$

$$\left\{ \begin{array}{l} 0 \leq \mu_1^{\text{min}} \perp (P_{\text{GT}}^{t,i} - P_{\text{GT}}^{\text{min}}) \geq 0, 0 \leq \mu_1^{\text{max}} \perp (P_{\text{GT}}^{\text{max}} - P_{\text{GT}}^{t,i}) \geq 0 \\ 0 \leq \mu_2^{\text{min}} \perp (Q_{\text{AC}}^{t,i} - Q_{\text{AC}}^{\text{min}}) \geq 0, 0 \leq \mu_2^{\text{max}} \perp (Q_{\text{AC}}^{\text{max}} - Q_{\text{AC}}^{t,i}) \geq 0 \\ 0 \leq \mu_3^{\text{min}} \perp (Q_{\text{ER}}^{t,i} - Q_{\text{ER}}^{\text{min}}) \geq 0, 0 \leq \mu_3^{\text{max}} \perp (Q_{\text{ER}}^{\text{max}} - Q_{\text{ER}}^{t,i}) \geq 0 \\ 0 \leq \mu_4^{\text{min}} \perp (Q_{\text{GB}}^{t,i} - Q_{\text{GB}}^{\text{min}}) \geq 0, 0 \leq \mu_4^{\text{max}} \perp (Q_{\text{GB}}^{\text{max}} - Q_{\text{GB}}^{t,i}) \geq 0 \\ 0 \leq \mu_5^{\text{min}} \perp (Q_{\text{HE}}^{t,i} - Q_{\text{HE}}^{\text{min}}) \geq 0, 0 \leq \mu_5^{\text{max}} \perp (Q_{\text{HE}}^{\text{max}} - Q_{\text{HE}}^{t,i}) \geq 0 \\ 0 \leq \mu_6^{\text{min}} \perp P_{\text{grid}}^{t,i} \geq 0, 0 \leq \mu_6^{\text{max}} \perp (P_{\text{grid}}^{\text{max}} - P_{\text{grid}}^{t,i}) \geq 0 \\ 0 \leq \mu_7^{\text{min}} \perp P_{\text{mg},s}^{t,i} \geq 0, 0 \leq \mu_7^{\text{max}} \perp (P_{\text{mg}}^{\text{max}} \cdot U_{\text{sale}}^{t,i} - P_{\text{mg},s}^{t,i}) \geq 0 \\ 0 \leq \mu_8^{\text{min}} \perp P_{\text{mg},b}^{t,i} \geq 0, 0 \leq \mu_8^{\text{max}} \perp (P_{\text{mg}}^{\text{max}} \cdot U_{\text{buy}}^{t,i} - P_{\text{mg},b}^{t,i}) \geq 0 \\ 0 \leq \mu_9^{\text{max}} \perp (1 - U_{\text{sale}}^{t,i} - U_{\text{buy}}^{t,i}) \geq 0 \\ 0 \leq \mu_{10}^{\text{min}} \perp Q_{\text{mg},s}^{t,i} \geq 0 \\ 0 \leq \mu_{11}^{\text{min}} \perp Q_{\text{mg},b}^{t,i} \geq 0, 0 \leq \mu_{11}^{\text{max}} \perp (Q_{\text{mg}}^{\text{max}} \cdot V_{\text{buy}}^{t,i} - Q_{\text{mg},b}^{t,i}) \geq 0 \\ 0 \leq \mu_{12}^{\text{max}} \perp (1 - V_{\text{sale}}^{t,i} - V_{\text{buy}}^{t,i}) \geq 0 \end{array} \right. \quad (40)$$

Step 3: Based on the transformed single-level model, as shown in Equations (39) and (40), the Big-M method is used to introduce 0–1 variables to transform the nonlinear constraints in the model into mixed-integer linear constraints, for example:

$$0 \leq \mu_1^{\text{min}} \leq M_{\mu}^{\text{min}} v^{\text{min}} \quad (41)$$

$$0 \leq P_{\text{GT}}^{t,i} - P_{\text{GT}}^{\text{min}} \leq M_{\mu}^{\text{min}} (1 - v^{\text{min}}) \quad (42)$$

where M_{μ}^{min} is a sufficiently large constant; v^{min} is a binary variable.

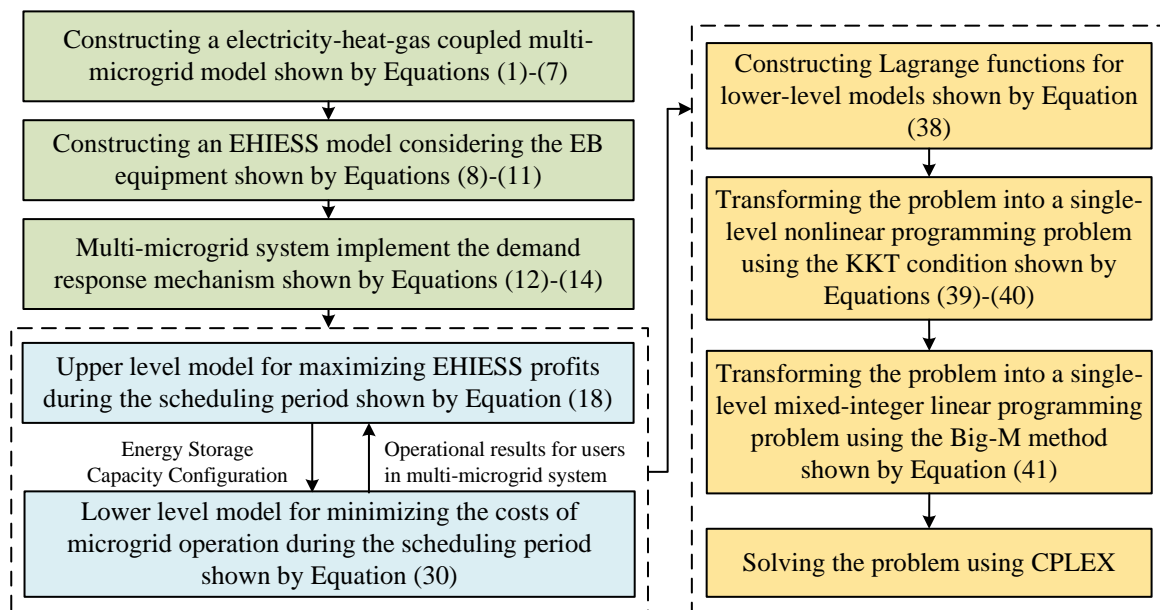


Figure 3. Schematic diagram of the solution process.

4. Simulation Analysis

4.1. Parameter Settings

The multi-microgrid system in this paper consists of three microgrids equipped with CCHP, wind turbine and photovoltaic, and is connected to EHIESS consisting of ESU, TSU and EB. The predicted output data of wind turbine and photovoltaic for the three microgrids in summer and winter, as well as three loads demands of electricity, heat and cooling are shown in Figure 4 [36], where MG 3 is not equipped with WT. The scheduling period is set to 24 h. The time-of-use price after DR and the transaction price between the multi-microgrid system and ESU are shown in Table 2 [36]. The detailed operation parameters of energy conversion equipment are shown in Table 3 [37]. The power cost of ESU and TSU is \$281.66/kW and \$70.40/kW (The original data used CNY as the unit, for reading convenience, this paper uses the RMB-USD exchange rate of 12 October 2024 to convert the unit to USD. It will not be separately noted later.). The capacity of ESU and TSU cost is \$267.11/kWh and \$26.753/kWh [37]. The service fees charged by EHIESS is \$0.0014/kW. The price of natural gas is taken as 0.31 \$/m³. The price of heat sold to the TSU is \$0.014/kWh, and the price of heat purchased from the TSU is \$0.056/kWh.

Table 2. Time-of-use price parameters.

Time Period		Electricity Price(/\$/kWh)		
		Upstream Network Electricity Price	ESU's Selling Electricity Price	ESU's Purchasing Electricity Price
Peak period	08:00–13:00	0.19	0.16	0.13
	16:00–21:00			
Flat period	13:00–16:00	0.12	0.11	0.08
	21:00–24:00			
Valley period	00:00–08:00	0.05	0.06	0.03

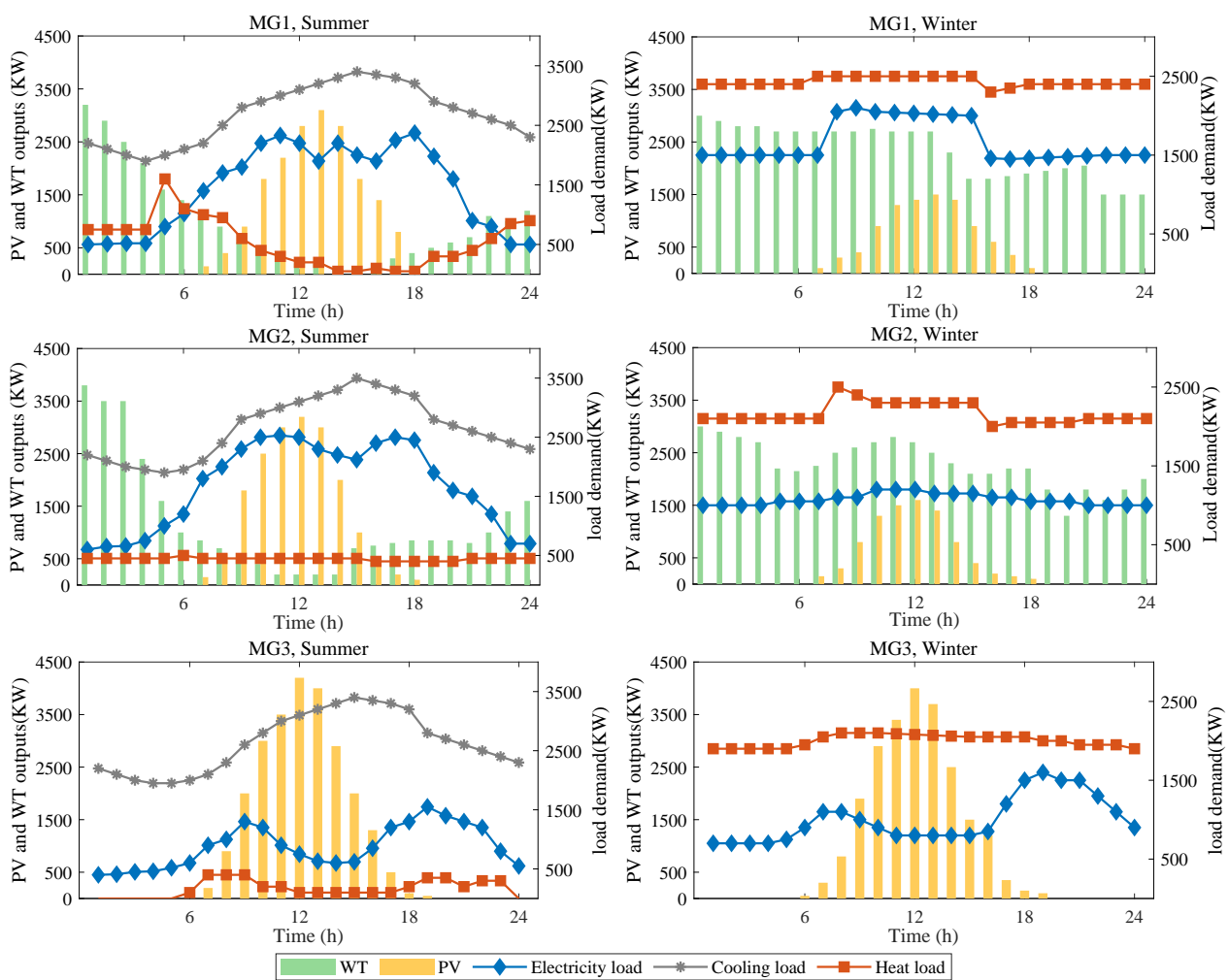


Figure 4. Loads demands and predicted power generation of PV and WT in multi-microgrid system.

Table 3. Equipment parameters of the microgrid.

Parameters	Numerical Value
Electricity generation efficiency of gas turbine, η_{GT}	0.3
Electricity-to-heat ratio of gas turbine, γ_{GT}	1.47
Heat generation efficiency of gas boiler, η_{GB}	0.9
Heat absorption efficiency of WHB, η_{WHB}	0.8
Cooling efficiency of electric refrigerator, η_{ER}	4
Energy utilization rates of heat exchange, η_{HE}	0.9
Energy utilization rates of LBAC, η_{AC}	1.2
Electricity charging and discharging efficiencies of ESU	0.95
Heat charging and discharging efficiencies of TSU	0.95
Electricity-heat conversion efficiency of EB, η_{EB}	3
Energy multiplication factor of ESU, η_{ESU}	2.7
Energy multiplication factor of TSU, η_{TSU}	0.2
Maximum power of gas turbine, kW	3000
Maximum power of LBAC, kW	4000
Maximum power of electric refrigerator, kW	4000
Maximum power of gas boiler, kW	4000
Maximum power of heat exchange, kW	4000
Maximum power transaction of multi-microgrid system, kW	4000

4.2. Analysis of the Operation and Economic Scheduling of EHI ESS

In this paper, the impact of EHI ESS on the multi-microgrid system operation is comparatively analyzed by setting up the following three cases.

Case 1: The multi-microgrid system is connected only to ESU, with ESU providing the electricity storage service.

Case 2: The multi-microgrid system is connected to ESU and TSU, with ESU and TSU providing electricity and heat storage service, respectively.

Case 3: The multi-microgrid system is connected to EHI ESS, which includes ESU, TSU, and EB that can provide electricity and heat storage services, and realize electricity-heat coupling.

Table 4 shows the operation costs of the multi-microgrid system and the profits of EHI ESS for three different cases. From Table 4, we can see that the profits of EHI ESS keep increasing while the operation costs of the multi-microgrid system keep decreasing after adding TSU and EB devices in both summer and winter cases. Figure 5 reflects the charging and discharging energy of EHI ESS under three cases in summer, from which we can see that the multi-microgrid system in Case 1 sells electricity to EHI ESS during the lower load hours of 01:00–4:00 and 10:00–14:00, and purchases electricity from EHI ESS during the higher load hours of 06:00–9:00 and 16:00–19:00. The addition of the TSU in Case 2 allows the multi-microgrid system to trade heat with EHIES. TSU can store excess heat to reduce heat waste, which reduces the heat production of CCHP in multi-microgrid system fairly, and reduces the operation costs of the multi-microgrid system in summer from \$10,352.25 to \$9884.21 in Case 1. Meanwhile, the operation costs of the multi-microgrid system in winter decreases from \$36,745.27 to \$35,291.77, and the profits of EHI ESS in winter rises from \$3754.61 to \$6397.26. In Case 3, TSU is in heat discharging state for 23 h during the scheduling period, which is due to the input of EB equipment makes part of the electricity in ESU converted into heat. At this time, the profits of EHI ESS in Case 3 are \$1933.88 and \$8825.53 in summer and winter, respectively, which are 12.25% and 37.96% higher compared to Case 2. The operation of EHI ESS alleviates the heat production pressure and dependence on natural gas of gas turbine and gas boiler in multi-microgrid system, and realizes synergistic operation and complementary advantages between different microgrids.

Table 4. Profits of EHI ESS and operation cost of multi-microgrid system in summer and winter.

Season	Case	Profits of EHI ESS/\$	Operation Costs of the Multi-Microgrid System/\$
Summer	1	489.27	10,352.25
	2	1722.87	9884.21
	3	1933.88	7799.96
Winter	1	3754.61	36,745.27
	2	6397.26	35,291.77
	3	8825.53	26,628.18

Table 5 reflects the energy purchases from upper level energy grid by multi-microgrid system under Case 2 and Case 3. As can be seen from Table 5, the addition of the EB results in a significant increase of the purchased power of the multi-microgrid system both in summer and winter, whereas the purchased natural gas of the multi-microgrid system has a significant decrease in summer and winter by 6757.1 kWh and 41,766.6 kWh, respectively. The inclusion of EB realizes the coupled utilization of ESU and TSU so that the dependence of the multi-microgrid system on the energy storage has reduced. Besides, because of the higher construction cost of ESU relative to TSU, the configuration capacity of the ESU is reduced accordingly. Meanwhile, the multi-microgrid system in Case 3 has lower energy purchase costs in summer and winter compared to Case 2. The input of EB strengthens the energy interaction between different microgrids, and improves the utilization rate of the

energy storage equipment in EHISS, which significantly improves the economics of both the multi-microgrid system and EHISS.

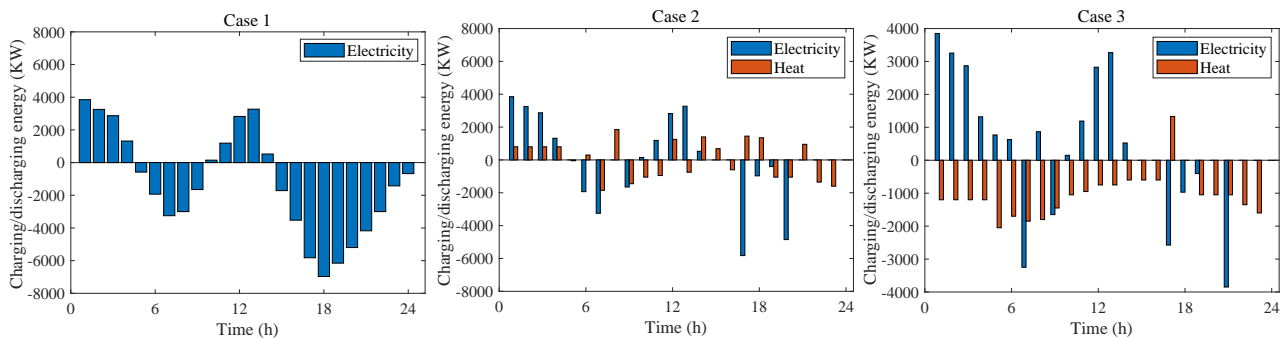


Figure 5. Charging and discharging energy EHISS for Case 1 to Case 3 in summer.

Table 5. Energy purchase from upper-level energy grid for Case 2 and Case 3.

Season	Case2			Case3		
	Electricity Purchase /kWh	Natural Gas Purchase /kWh	Cost of Energy Purchase /\$	Electricity Purchase /kWh	Natural Gas Purchase /kWh	Cost of Energy Purchase /\$
Summer	8301.7	14,335.4	5609.60	14,059.3	7578.3	4880.98
Winter	57,091.5	62,568.8	27,420.73	79,857.7	20,802.2	13,092.99

In order to further evaluate the effectiveness of the shared energy storage optimal configuration model proposed in this paper, simulations are conducted in two scenarios of fixed energy storage capacity and optimal configuration of energy storage capacity in EHISS. Summer load demands, wind and photovoltaic data of three microgrids are selected, and the optimal operation of EHISS with the TSU capacity set to 10,000, 11,000, 12,000 kWh and TSU capacity set to 8000, 8500, 9000 kWh respectively is solved to compare with the optimal configuration scenarios of EHISS, and the obtained results are shown in Table 6. When the ESU and TSU capacities are set to 10,000 kWh and 8000 kWh, respectively, EHISS cannot guarantee the stable supply of electricity and heat to multi-microgrid systems, and the optimal solution cannot be obtained in this case. With the gradual increase of ESU and TSU capacity configurations, the energy storage construction and maintenance cost of EHISS increases accordingly. Meanwhile, we find that as the storage capacity configuration increases, the storage capacity utilization rate gradually decreases, and the operation revenue of EHISS during the scheduling period also gradually decreases.

Table 6. Operation results of EHISS under fixed capacity configuration and optimal capacity configuration scenarios for energy storage unit.

Scenario	ESU Capacity/kWh	TSU Capacity/kWh	p_{es}^{max}/kW	Q_{es}^{max}/kW	Profit of EHISS/\$
Scenario 1	10,000	8000	-	-	-
ine Scenario 2	11,000	8500	4126.34	2833.33	1683.25
Scenario 3	12,000	9000	4501.46	3000	1654.28
Optimal configuration	10,263.33	8290.79	3850	2763.60	1933.88

4.3. Analysis of User-Side Price-Based Demand Response

Figure 6 shows the power balance and upstream network electricity price considering DR in Case 3. In the multi-microgrid system, the electricity is mainly supplied by PV, WT, and CCHP. The multi-microgrid system can trade energy with EHIESS, and each microgrid transmits energy to each other through EHIESS.

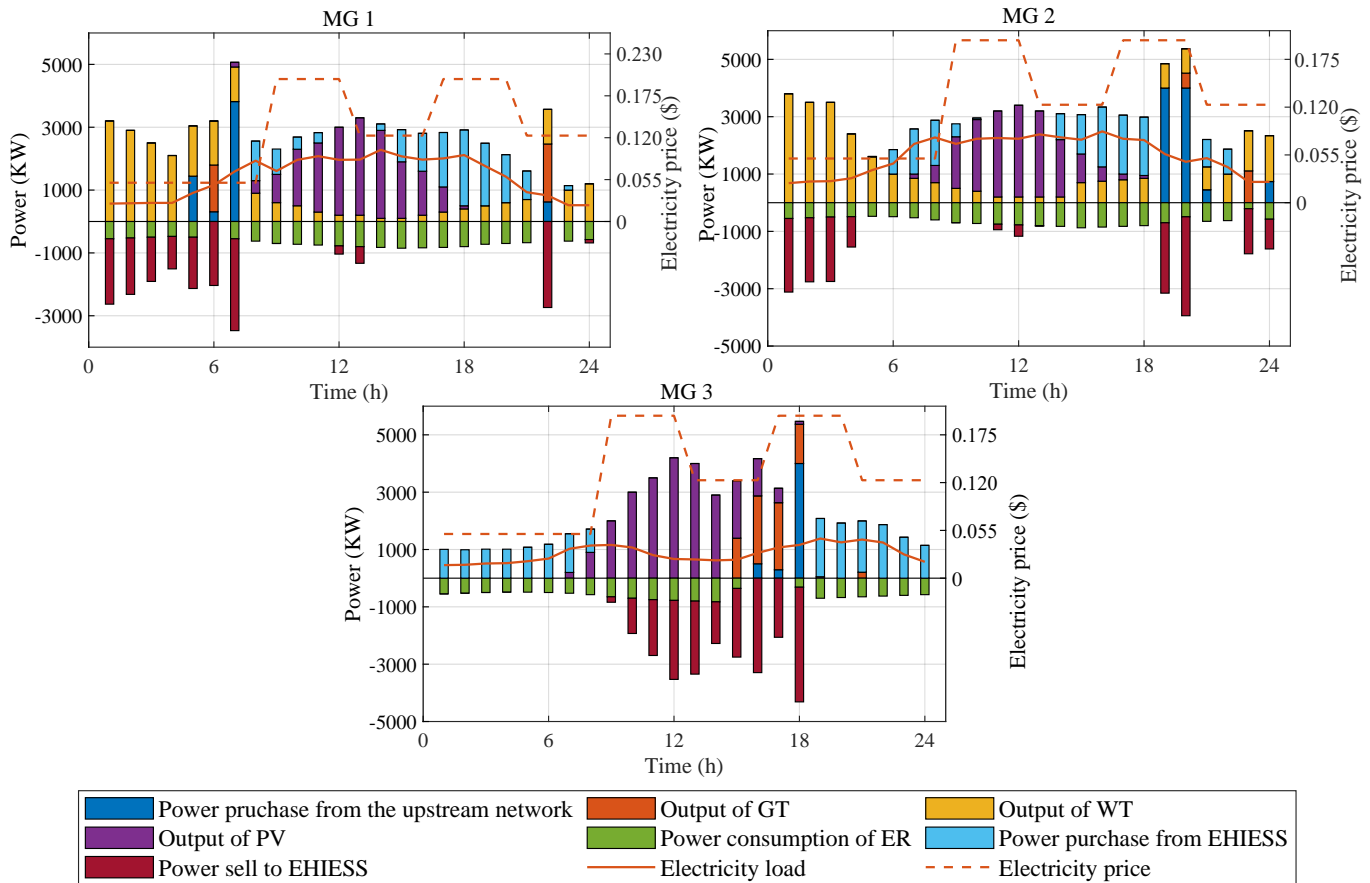


Figure 6. Power balance and upstream network electricity price considering DR in Case 3.

As we can see in Figure 6, after the introduction of renewable energy generation in conjunction with CCHP and the consideration of DR, the power generation of the multi-microgrid system is more diversified, which effectively improves the flexibility of the operation of the multi-microgrid system. Among them, electricity generation of PV and WT in each MG can be completely consumed, while the stochastic problem of WT and PV generation can be solved by EHIESS. In addition, the time-of-use price can guide the trading behavior of the multi-microgrid system with EHIESS. Besides, the sum of electricity generated by PV and WT and the output of CCHP is much larger than the user’s demand from 01:00 to 08:00. In order to prevent the waste of energy, the time-of-use price can guide users to transfer their electricity consumption behavior to period 01:00–08:00. The three MGs transfer their loads from 01:00 to 08:00, which are 964.3 kW, 1198.1 kW and 655.8 kW, respectively, and the multi-microgrid system can sell surplus electricity to EHIESS to get profits. The 9:00–12:00 and 17:00–20:00 time periods are peak periods, during which DR can drive users to slash their electricity consumption behavior and prompt them to buy electricity from EHIESS, and the total load reduction of three MGs in peak periods are 120.5 kW, 131.6 kW, and 69.1 kW, respectively. The 13:00–16:00 and 21:00–24:00 time periods are the flat periods, and the multi-microgrid system can sell surplus electricity to EHIESS to gain profits. MG relies on the WT generation and electricity purchase from EHIESS to meet its own electricity load demands, and adjusts its electricity consumption behavior.

Table 7 reflects the operation situation of the multi-microgrid system before and after the implementation of DR in summer. From Table 6, it can be seen that the multi-microgrid system has better economic benefits after the implementation of DR, in which the operation cost of the multi-microgrid system is reduced by \$522.05. In addition, the peak-to-valley difference of electric loads in the multi-microgrid system is reduced after considering DR in the user side, which leads to smoother load curves and more stable operation of the multi-microgrid system. This follows the fact that the implementation of DR prompts the users to shift the electricity load from the peak hours to other hours, which facilitates peak shaving and valley filling, thus reducing the value of the electricity load in peak periods. Finally, the capacity of ESU is reduced from 10,263.33 kWh to 9730.80 kWh after the implementation of DR in the user side. The implementation of DR makes the generation of each microgrid more compatible with the changes of electricity price, which reduces the generation of excess electricity in certain extent, so that the transactions of multi-microgrid system and EHIESS are reduced accordingly, and reduces the required capacity of the ESU.

Table 7. The operation situation of the multi-microgrid system before and after DR in summer.

Scenario	Operation Costs of Multiple Microgrids/\$	Profits of EHIESS/\$	Peak-to-Valley Difference in Electricity Loads/kW			ESU Capacity Configuration /kWh
			MG1	MG2	MG3	
Before DR	7799.96	1933.88	1830.00	1930.00	1150.00	10,263.33
After DR	7277.91	1687.40	1762.06	1804.60	927.48	9730.80

User satisfaction is an essential consideration in the operation of the multi-microgrid system, which is related to the changing magnitude of SL and CL. According to Ref. [38], the user satisfaction, S_u , can be expressed as follows:

$$S_u = \frac{P_L^0 - |\Delta P_{CL}^t| - |\Delta P_{SL}^t|}{P_L^0} \times 100\% \quad (43)$$

Simulations are carried out for different load shares of CL and SL in total load demands to analyze the impact on the system's operation. Figure 7 shows the operation costs of the multi-microgrid system and the customer satisfaction in the case of CL and SL each with a share of 5% to 25%. From Figure 7, it can be seen that as the share of CL and SL increases, the operation costs of the multi-microgrid system gradually decreases from \$8558.33 to \$7369.94, and the customer satisfaction gradually decreases from 98.44% to 92.22%. With the total microgrid load demand remaining unchanged, the DR behavior of multi-microgrid system increases as the CL and SL share gradually increases, prompting more load shifting from the peak hours to the valley hours and reducing the operation costs of the multi-microgrid system. Whereas, price-based DR forces users to shift the time of electricity consumption, which is contrary to the customer's willingness, and thus the increase of CL and SL share reduces the customer satisfaction.

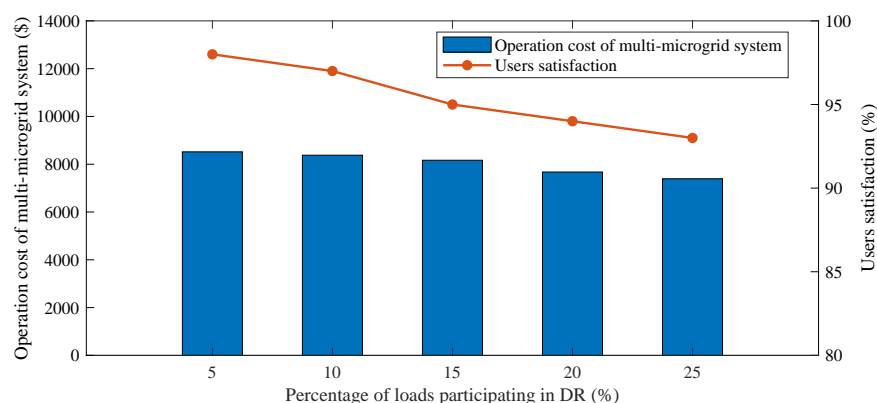


Figure 7. Operation costs and customer satisfaction of microgrids with different load shares after considering DR under Case3.

4.4. Analysis of Sensitivity

The variation range of variables (i.e., electricity price and load demands of multi-microgrid system, etc.) is set to -20% – 20% , based on Case 3 in summer, and the results of the sensitivity analysis of these variables on the results of the energy storage configuration, the EHIESS operation revenue, and the operation costs of multi-microgrid system are shown in Tables 8 and 9. As shown in Table 9, within the range of changes in electricity, with each 10% increase, EHIESS operation revenue and multi-microgrid system operation cost increase slightly, and ESU and TSU capacity configurations remain essentially unchanged. The sensitivity of electricity price to EHIESS operation revenue and operation cost of multi-microgrid system is relatively insignificant. For the load demand of multi-microgrid users, as shown in Table 9, with the loads changed by -20% , -10% , 10% , and 20% , the EHIESS operation revenue changed by -49.2% , -24.1% , 24.5% , and 46.9% , and the multi-microgrid system operation cost increased by -37.7% , -17.3% , 19.3% and 33.9% , respectively. As can be seen in Table 9, the sensitivity of the change in load demand to the EHIESS operation revenue and the operation cost of multi-microgrid system is more significant.

Table 8. Influence of electricity price changes on operation results.

Electricity Price	Profits of EHIESS/\$	Operation Costs of Multi-Microgrid System/\$	ESU Capacity/kWh	TSU Capacity/kWh
-20%	1930.89	7310.84	10,263.33	9090.23
-10%	1931.56	7484.73	10,263.33	8290.79
0%	1933.88	7799.96	10,263.33	8290.79
10%	1935.75	8537.65	10,263.33	8170.36
20%	1938.23	8620.57	10,263.33	8170.36

Table 9. Influence of load demand changes on operation results.

Electricity Price	Profits of EHIESS/\$	Operation Costs of Multi-Microgrid System/\$	ESU Capacity/kWh	TSU Capacity/kWh
-20%	981.87	4860.88	12,355.98	12,273.05
-10%	1468.40	6457.18	10,765.48	9090.23
0%	1933.88	7799.96	10,263.33	8290.79
10%	2408.21	9308.22	9863.46	6560.43
20%	2840.66	10,442.00	9463.59	6036.65

4.5. Analysis of Comparison of Solution Methods

In order to verify the effectiveness of the KKT condition and Big-M optimization method used in this paper to solve the bi-level planning problem of optimizing the shared energy storage configuration of multi-microgrid system, the computational efficiencies of the transformed single-level model and the original bi-level model are compared and analyzed. The computational results of the two solution methods are shown in Table 10. Since the original bi-level optimization model is a nonlinear optimization model, it is necessary to adopt corresponding intelligent algorithms to solve iteratively, which is easy to fall into the local optimal solution and consumes a large amount of computing time. It can be seen from the table that the computational time is significantly reduced after transforming into single-level optimization model, which also leads to a relative increase in the operation revenue of EHIESS and a decrease in the operation cost of multi-microgrid users.

Table 10. Calculation results of two solution methods.

Season	Calculation Time/s	Profits of EHIESS/\$	Operation Costs of Multi-Microgrid System/\$
Original bi-level model	319.6	1876.45	8209.87
Single-level model	8.6	1933.88	7799.96

5. Conclusions

In this paper, a bi-level optimization model considering EHIESS capacity configuration and optimal scheduling of multi-microgrid system is proposed to maximize the profits of EHIESS and minimize the operation costs of multi-microgrid system. The case studies demonstrate the effectiveness of the proposed methodology in solving the problem of high cost and low utilization of energy storage equipment configuration in multi-microgrid system. The main research results are as follows:

The introduction of EB in EHIESS makes the electricity-heat coupling in EHIESS more flexible, significantly improves the energy utilization rate of the storage equipment, and brings better economic benefits to the multi-microgrid system. Compared to the scenario considering only the separate configuration of electricity and heat energy storage, the addition of EB improves the total profits of EHIESS in one scheduling period by \$211.01 and \$2428.27 in summer and winter, respectively, and reduces the total operation costs of the multi-microgrid system by \$2084.25 and \$8663.59, respectively. In addition, DR provides an effective solution to the problem of load demand uncertainty on the user side, and users adjust their own electricity consumption behavior based on time-of-use price, which smooths out load fluctuations and effectively improves the flexibility of the operation of the multi-microgrid system. After the implementation of the price-based DR mechanism, the configuration of ESU and TSU in EHIESS is reduced by 532.53 kW, which further improves the economic efficiency of multi-microgrid system and EHIESS. In this case, the total operation cost of multi-microgrid system is reduced by \$522.05.

This paper focuses on multi-microgrid shared energy storage systems, and future research can be extended to a wider range of application scenarios and consider different sizes and types of energy systems to provide broader application guidance and decision support. The main limitation of the proposed model is that it does not fully analyze the impact of renewable energy uncertainty on shared storage capacity allocation. In future research work, we will further consider the issue of evaluating the impact of multiple uncertainties, such as wind power and photovoltaic, on multi-microgrid shared energy storage systems. Besides, cost sharing between EHIESS and multi-microgrid system users will be further studied and explored, and game-based pricing mechanisms for service fees will be discussed.

Author Contributions: Conceptualization, Y.L.; methodology, Y.L.; software, Y.L., Z.W. and J.G.; validation, Y.L.; formal analysis, Z.D.; investigation, J.Z.; resources, W.Y.; writing—original draft preparation, Y.L.; writing—review and editing, Y.L. and Z.D.; visualization, Z.W. and J.G.; project administration, Z.D.; funding acquisition, Z.D. All authors have read and agreed to the published version of the manuscript.

Funding: This work was supported by National Natural Science Foundation of China under grant 52005306, Natural Science Foundation of Shandong Province under grant ZR2020QE220.

Institutional Review Board Statement: Not applicable.

Informed Consent Statement: Informed consent was collected from all participants in this study.

Data Availability Statement: Data is contained within the article.

Conflicts of Interest: Jingwei Zhao is from State Power Investment Corporation Haiyang Offshore Wind Power Co., Ltd. They declared no conflict of interest.

Nomenclature

Acronyms

CCHP	combined cooling heating and power
DR	demand response
EB	electric boiler
EHIESS	electricity-heat integrated energy storage supplier
ESU	electricity storage unit
KKT	Karush-Kuhn-Tucker
LBAC	lithium bromide absorption chiller
TSU	thermal storage unit
WHB	waste heat boiler

Variables

E^t	the electricity stored in ESU during hour t , MW
H^t	the heat stored in TSU during hour t , MW
P_{ch}^t	the electricity purchased by ESU during hour t , MW
P_{dis}^t	the electricity sold by ESU during hour t , MW
P_{EB}^t	the power consumption of EB during hour t , MW
$P_{grid}^{t,i}$	the electricity purchased of MG i from the upstream network during hour t , MW
$P_{GT}^{t,i}$	the electricity generated by gas turbine of MG i during hour t , MW
$P_{mg,b}^{t,i}$	the electricity purchased from EHIESS of MG i during hour t , MW
$P_{mg,s}^{t,i}$	the electricity sold to EHIESS of MG i during hour t , MW
$Q_{AC}^{t,i}$	the cooling output of LBAC in MG i during hour t , MW
Q_{ch}^t	the heat purchased by TSU during hour t , MW
Q_{dis}^t	the heat sold by TSU during hour t , MW
$Q_{EB}^{t,i}$	the heat produced by EB during hour t , MW
$Q_{ER}^{t,i}$	the cooling output of ER in MG i during hour t , MW
$Q_{GB}^{t,i}$	the heat generation of gas boiler in MG i during hour t , MW
$Q_{GT}^{t,i}$	the heat generation of gas turbine in MG i during hour t , MW
$Q_{HE}^{t,i}$	the heat output of heat exchange in MG i during hour t , MW
$Q_{mg,b}^{t,i}$	the heat purchased from EHIESS of MG i during hour t , MW
$Q_{mg,s}^{t,i}$	the heat sold to EHIESS of MG i during hour t , MW
$Q_{WHB}^{t,i}$	the heat absorbed by WHB of MG i during hour t , MW
$V_{GB}^{t,i}$	the gas consumption volume of gas boiler in MG i during hour t , MW
$V_{GT}^{t,i}$	the gas consumption volume of gas turbine in MG i during hour t , MW
ΔP_{CL}^t	the changes of curtailable load after DR during hour t , MW
ΔP_{SL}^t	the changes of shiftable load after DR during hour t , MW

Parameters

L_{gas}	the heat value of natural gas, kWh/m ³
η_{AC}	the heat utilization rate of LBAC
η_{EB}	the conversion efficiency of EB
η_{ER}	the cooling efficiency of electric refrigerator
η_{GB}	the heat generation efficiency of gas boiler
η_{GT}	the electricity generation efficiency of gas turbine
η_{HE}	the heat utilization rate of heat exchange
η_{WHB}	the heat absorption efficiency of WHB
η_{abs}	the charging efficiency of ESU
η_{re}	the discharging efficiency of ESU
ω_{abs}	the charging efficiency of TSU
ω_{re}	the discharging efficiency of TSU
γ_{GT}	the heat generation efficiency of gas turbine
λ^t	the price of electricity purchased from ESU during hour t , CNY/MW
φ^t	the price of heat purchased from TSU during hour t , CNY/MW
δ^t	the price of electricity sold to ESU during hour t , CNY/MW
γ^t	the price of heat sold to TSU during hour t , CNY/MW
θ^t	the price of service fees received by EHIESS during hour t , CNY/MW
τ_{grid}^t	the electricity price of the upstream network, CNY/MW
τ_{gas}^t	the price of natural gas, CNY/m ³

References

- Dalala, Z.; Al-Omari, M.; Al-Addous, M.; Bdour, M.; Al-Khasawneh, Y.; Alkasrawi, M. Increased renewable energy penetration in national electrical grids constraints and solutions. *Energy* **2022**, *246*, 123361. [\[CrossRef\]](#)
- Li, Y.; Wei, Y.; Zhu, F.; Du, J.; Zhao, Z.; Ouyang, M. The path enabling storage of renewable energy toward carbon neutralization in China. *Etransportation* **2023**, *16*, 100226. [\[CrossRef\]](#)
- Ranjan, M.; Shankar, R. A literature survey on load frequency control considering renewable energy integration in power system: Recent trends and future prospects. *J. Energy Storage* **2022**, *45*, 103717. [\[CrossRef\]](#)
- Thirunavukkarasu, M.; Sawle, Y.; Lala, H. A comprehensive review on optimization of hybrid renewable energy systems using various optimization techniques. *Renew. Sustain. Energy Rev.* **2023**, *176*, 113192. [\[CrossRef\]](#)
- Zhong, X.; Zhong, W.; Liu, Y.; Yang, C.; Xie, S. Optimal energy management for multi-energy multi-microgrid networks considering carbon emission limitations. *Energy* **2022**, *246*, 123428. [\[CrossRef\]](#)
- Zhou, B.; Zou, J.; Chung, C.Y.; Wang, H.; Liu, N.; Voropai, N.; Xu, D. Multi-microgrid energy management systems: Architecture, communication, and scheduling strategies. *J. Mod. Power Syst. Clean Energy* **2021**, *9*, 463–476. [\[CrossRef\]](#)
- Xu, J.; Yi, Y. Multi-microgrid low-carbon economy operation strategy considering both source and load uncertainty: A Nash bargaining approach. *Energy* **2023**, *263*, 125712. [\[CrossRef\]](#)
- Zhao, J.; Wang, W.; Guo, C. Hierarchical optimal configuration of multi-energy microgrids system considering energy management in electricity market environment. *Int. J. Electr. Power Energy Syst.* **2023**, *144*, 108572. [\[CrossRef\]](#)
- Azizivahed, A.; Gholami, K.; Arefi, A.; Li, L.; Arif, M.; Haque, M. Stochastic scheduling of energy sharing in reconfigurable multi-microgrid systems in the presence of vehicle-to-grid technology. *Electr. Power Syst. Res.* **2024**, *231*, 110285. [\[CrossRef\]](#)
- Lei, L.; Wu, N. An optimal scheduling strategy for electricity-thermal synergy and complementarity among multi-microgrid based on cooperative games. *Renew. Energy* **2024**, *237*, 121575. [\[CrossRef\]](#)
- Jani, A.; Jadid, S. Two-stage energy scheduling framework for multi-microgrid system in market environment. *Appl. Energy* **2023**, *336*, 120683. [\[CrossRef\]](#)
- Carvalho, C.; Jalil-Vega, F.; Moreno, R. A multi-energy multi-microgrid system planning model for decarbonisation and decontamination of isolated systems. *Appl. Energy* **2023**, *343*, 121143. [\[CrossRef\]](#)
- Shi, Z.; Zhang, T.; Liu, Y.; Feng, Y.; Wang, R.; Huang, S. Optimal design and operation of islanded multi-microgrid system with distributionally robust optimization. *Electr. Power Syst. Res.* **2023**, *221*, 109437. [\[CrossRef\]](#)
- Numan, M.; Baig, M.F.; Yousif, M. Reliability evaluation of energy storage systems combined with other grid flexibility options: A review. *J. Energy Storage* **2023**, *63*, 107022.
- Li, L.; Peng, K.; Yang, X.; Liu, K. Coordinated design of multi-stakeholder community energy systems and shared energy storage under uncertain supply and demand: A game theoretical approach. *Sustain. Cities Soc.* **2024**, *100*, 105028. [\[CrossRef\]](#)
- Hu, J.; Wang, Y.; Dong, L. Low carbon-oriented planning of shared energy storage station for multiple integrated energy systems considering energy-carbon flow and carbon emission reduction. *Energy* **2024**, *290*, 130139. [\[CrossRef\]](#)
- Wang, Q.; Zhang, X.; Yi, C.; Li, Z.; Xu, D. A novel shared energy storage planning method considering the correlation of renewable uncertainties on the supply side. *IEEE Trans. Sustain. Energy* **2022**, *13*, 2051–2063. [\[CrossRef\]](#)

18. Han, J.; Fang, Y.; Li, Y.; Du, E.; Zhang, N. Optimal planning of multi-microgrid system with shared energy storage based on capacity leasing and energy sharing. In *IEEE Transactions on Smart Grid*; IEEE: Piscataway, NJ, USA, 2024.
19. Zheng, B.; Wei, W.; Chen, Y.; Wu, Q.; Mei, S. A peer-to-peer energy trading market embedded with residential shared energy storage units. *Appl. Energy* **2022**, *308*, 118400. [[CrossRef](#)]
20. Han, O.; Ding, T.; Zhang, X.; Mu, C.; He, X.; Zhang, H. A shared energy storage business model for data center clusters considering renewable energy uncertainties. *Renew. Energy* **2023**, *202*, 1273–1290. [[CrossRef](#)]
21. Zhang, X.; Wang, Z.; Liao, H.; Zhou, Z.; Ma, X.; Yin, X.; Wang, Z.; Liu, Y.; Lu, Z.; Lv, G. Optimal capacity planning and operation of shared energy storage system for large-scale photovoltaic integrated 5G base stations. *Int. J. Electr. Power Energy Syst.* **2023**, *147*, 108816. [[CrossRef](#)]
22. Dong, H.; Fu, Y.; Jia, Q.; Wen, X. Optimal dispatch of integrated energy microgrid considering hybrid structured electric-thermal energy storage. *Renew. Energy* **2022**, *199*, 628–639. [[CrossRef](#)]
23. Pradeep, N.; Reddy, K. Design and investigation of solar cogeneration system with packed bed thermal energy storage for ceramic industry. *Renew. Energy* **2022**, *192*, 243–263. [[CrossRef](#)]
24. He, Y.; Guo, S.; Zhou, J.; Ye, J.; Huang, J.; Zheng, K. Multi-objective planning-operation co-optimization of renewable energy system with hybrid energy storages. *Renew. Energy* **2022**, *184*, 776–790. [[CrossRef](#)]
25. Zeng, H.; Shao, B.; Dai, H.; Tian, N.; Zhao, W. Incentive-based demand response strategies for natural gas considering carbon emissions and load volatility. *Appl. Energy* **2023**, *348*, 121541. [[CrossRef](#)]
26. Dey, B.; Misra, S.; Marquez, F.P.G. Microgrid system energy management with demand response program for clean and economical operation. *Appl. Energy* **2023**, *334*, 120717. [[CrossRef](#)]
27. Tostado-Véliz, M.; Kamel, S.; Aymen, F.; Jordehi, A.R.; Jurado, F. A Stochastic-IGDT model for energy management in isolated microgrids considering failures and demand response. *Appl. Energy* **2022**, *317*, 119162. [[CrossRef](#)]
28. Yang, P.; Jiang, H.; Liu, C.; Kang, L.; Wang, C. Coordinated optimization scheduling operation of integrated energy system considering demand response and carbon trading mechanism. *Int. J. Electr. Power Energy Syst.* **2023**, *147*, 108902. [[CrossRef](#)]
29. Saberi-Beglar, K.; Zare, K.; Marzband, M.; Nojavan, S. Risk-embedded scheduling of a CCHP integrated with electric vehicle parking lot in a residential energy hub considering flexible thermal and electrical loads. *Appl. Energy* **2023**, *329*, 120265. [[CrossRef](#)]
30. Alfaverh, F.; Denai, M.; Sun, Y. A dynamic peer-to-peer electricity market model for a community microgrid with price-based demand response. *IEEE Trans. Smart Grid* **2023**, *14*, 3976–3991. [[CrossRef](#)]
31. Kong, X.; Wang, Z.; Liu, C.; Zhang, D.; Gao, H. Refined peak shaving potential assessment and differentiated decision-making method for user load in virtual power plants. *Appl. Energy* **2023**, *334*, 120609. [[CrossRef](#)]
32. Alikhani, M.; Moghaddam, M.P.; Moazzen, F.; Azadi, A. Optimal implementation of consumer demand response program with consideration of uncertain generation in a microgrid. *Electr. Power Syst. Res.* **2023**, *225*, 109859. [[CrossRef](#)]
33. Fang, X.; Li, F.; Wei, Y.; Cui, H. Strategic scheduling of energy storage for load serving entities in locational marginal pricing market. *IET Gener. Trans. Dis.* **2016**, *10*, 1258–1267. [[CrossRef](#)]
34. Li, L.; Xu, Q.; Wang, X.; Ling, J.; Sun, H. Optimal economic scheduling of industrial customers on the basis of sharing energy-storage station. *Electr. Power Constr.* **2020**, *41*, 100–107. (In Chinese)
35. Zhang, B.; Li, Q.; Wang, L.; Feng, W. Robust optimization for energy transactions in multi-microgrids under uncertainty. *Appl. Energy* **2018**, *217*, 346–360. [[CrossRef](#)]
36. Cao, W.; Xiao, J.W.; Cui, S.C.; Liu, X.K. An efficient and economical storage and energy sharing model for multiple multi-energy microgrids. *Energy* **2022**, *244*, 123124. [[CrossRef](#)]
37. Guo, Y.; Wang, C.; Shi, Y.; Guo, C.; Shang, J.; Yang, X. Comprehensive optimization configuration of electric and thermal cloud energy storage in regional integrated energy system. *Power Syst. Technol.* **2020**, *44*, 1611–1621. (In Chinese)
38. Hu, G.; Yan, Y.; Wu, H.; Jin, P. Emergency load control strategy and terminal implementation for distribution network based on collaboration of main grid and distribution network. *Autom. Electr. Power Syst.* **2022**, *46*, 180–187.

Disclaimer/Publisher’s Note: The statements, opinions and data contained in all publications are solely those of the individual author(s) and contributor(s) and not of MDPI and/or the editor(s). MDPI and/or the editor(s) disclaim responsibility for any injury to people or property resulting from any ideas, methods, instructions or products referred to in the content.